Chapter 11
Interfacing Single Quantum Dot Spins with Photons Using a Nanophotonic Cavity

Shuo Sun and Edo Waks

Abstract The spin of a single electron or hole trapped inside a quantum dot offers a promising quantum memory. These qubits are embedded in a host semiconductor material that can be directly patterned to form compact integrated nanophotonic devices. These devices efficiently interconnect single solid-state qubits with photons, a crucial requirement for quantum networks, quantum repeaters, and photonic quantum computation. This chapter reviews recent experimental progress towards achieving strong spin-photon interactions based on coupled quantum dot and nanophotonic cavity system. Especially we introduce a recent work that reports a coherent spin-photon quantum switch operating at the fundamental quantum limit, where a single photon flips the orientation of a quantum dot spin and the spin flips the polarization of the photon. These strong spin-photon interactions open up a promising direction for solid-state implementations of high-speed quantum networks and on-chip quantum photonic circuits using nanophotonic devices.

11.1 Introduction

Interactions between single spins and photons play a central role in the field of quantum information processing. Spin is a pristine quantum memory while photons are ideal carriers of quantum information. Efficient interfaces between these systems are essential for development of future quantum networks [1, 2] and distributed quantum computers [3]. They also enable critical functionalities such as entanglement distribution [4, 5], non-destructive qubit measurements [6–8], and strong photon-photon interactions for photonic quantum computation [9, 10].

S. Sun (✉) · E. Waks
Department of Electrical and Computer Engineering, Institute for Research in Electronics and Applied Physics (IREAP), and Joint Quantum Institute (JQI), University of Maryland, College Park, MD 20742, USA
e-mail: shuosun@umd.edu

E. Waks
e-mail: edowaks@umd.edu

P. Michler (ed.), *Quantum Dots for Quantum Information Technologies*, Nano-Optics and Nanophotonics, DOI 10.1007/978-3-319-56378-7_11

The spin of a singly charged quantum dot has attracted significant interests for implementing a spin-photon interface. This trapped spin system provides a promising quantum memory with microsecond coherence time [11, 12] and picosecond timescale single-qubit gates [12–17], enabling a large number of quantum operations prior to qubit decoherence. Furthermore, the spin ground states of the charged quantum dot are optically coupled to excited trion states that exhibit nearly radiatively limited emission [18]. These properties have enabled post-selected spin-photon entanglement [19–22], spin-photon teleportation [23], and spin-spin entanglement [24], which are essential capabilities for quantum networks.

Quantum dots are also embedded in a high dielectric solid-state substrate that can be directly patterned to form nanophotonic cavities that enhance light-matter interactions [25–28]. These devices can be integrated on-a-chip to attain a compact architecture for quantum circuits [29, 30]. Tremendous experimental progress has been made in the last decade using a quantum dot strongly coupled to a nanophotonic cavity, including cavity reflectivity control [31], ultrafast optical switch [32–34], single photon level nonlinearities [35–37], non-classical light generation [38, 39], and spin-exciton quantum logic operations [40]. The effort to integrate quantum dot spins with cavities has also experienced rapid progress. Several works demonstrated deterministic loading of a spin in a quantum dot coupled to a nanophotonic cavity [41–43], and more recently coherent control of the loaded spin [44] and spin-dependent Kerr rotation of photons [45, 46]. Very recently, a coherent quantum switch between a quantum dot spin and a photon has also been demonstrated [47].

In this chapter, we review recent experimental progress towards achieving strong spin-photon interactions based on coupled quantum dot and nanophotonic cavity system. This chapter is organized as follows. Section 11.2 provides a theoretical background for interfacing single spins and photons based on a cavity quantum electrodynamics (QED) system. Section 11.3 reviews the experimental efforts to integrate quantum dot spins with different nanophotonic cavities, including micropillar cavities and photonic crystal cavities. In Sect. 11.4, we focus on a recent experimental work that demonstrates a coherent spin-photon quantum switch, where through the mediation of a strongly coupled photonic crystal cavity, a single photon flips the orientation of a quantum dot spin and the spin flips the polarization of the photon. Section 11.5 concludes our discussion and provides outlook for future works.

11.2 Theoretical Background

In this section, we provide theoretical background on using a cavity QED system to interconnect an optical active qubit with photons. We focus our analysis on a generic system consisted of an optical active qubit coupled to an optical cavity, as shown in Fig. 11.1a. We assume that the qubit system has a λ-type energy structure as shown in Fig. 11.1b, with two ground states that form a stable spin qubit, denoted as $|\uparrow\rangle$ and $|\downarrow\rangle$, and one excited state $|e\rangle$ that gives rise to spin-dependent optical transitions

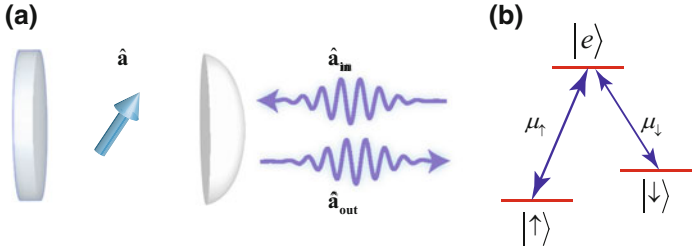

Fig. 11.1 Theoretical model for a generic cavity QED system composed of an optical active qubit coupled to an optical cavity. **a** A schematic cavity QED system. **b** Energy level structure of a generic optical active qubit system

$\mu_\uparrow$ and $\mu_\downarrow$ respectively. The spin-dependent optical transitions provide a mechanism to interconnect the spin qubit with photons. This energy structure exists in many qubit systems that are optically addressable, such as cold atoms, trapped ions, color centers, and charged quantum dots, and therefore represents a generic model.

In order to induce strong spin-photon interactions, we selectively couple the optical transition $\mu_\uparrow$ to a cavity mode, while decouple the other transition $\mu_\downarrow$ to the cavity, either by a large detuning or by selection rules if transition $\mu_\downarrow$ emits a photon with a different polarization than the cavity mode. In this configuration the coupling between the atom and the cavity depends on the spin state. The cavity thus exhibits spin-dependent reflection or transmission coefficients, enabling control of a reflected or transmitted photon by the spin qubit. In our model, we assume that the cavity field only couples to its reflective mode without loss of generality. In this case the spin only modulates the reflection coefficient of the cavity. Double-sided cavities would work similarly with minor modifications.

11.2.1 Calculation of Spin-Dependent Cavity Reflection Coefficients

We calculate the cavity reflection coefficients using cavity input-output formalism [48]. We define $\hat{\mathbf{a}}$ as the bosonic annihilation operator for the cavity field, and $\hat{\mathbf{a}}_{\mathbf{in}}$ and $\hat{\mathbf{a}}_{\mathbf{out}}$ as the operators for the cavity coupled incidence and reflection modes. These operators are related by the cavity input-output relation

$$\hat{\mathbf{a}}_{\mathbf{out}} = \hat{\mathbf{a}}_{\mathbf{in}} - \sqrt{\kappa_{ex}}\hat{\mathbf{a}}, \tag{11.1}$$

where κ_{ex} is the cavity energy decay rate to the reflection mode of the cavity.

In order to calculate the reflection coefficients, we need an expression for the cavity field operator $\hat{\mathbf{a}}$. We assume that the incident photon is quasi-monochromatic

with a frequency of ω. We express the Hamiltonian for the coupled atom and cavity system in the rotating reference frame with respect to ω, given by

$$\mathbf{H} = \hbar(\omega_c - \omega)\hat{\mathbf{a}}^\dagger\hat{\mathbf{a}} + \hbar(\omega_x - \omega)\hat{\sigma}_-^\dagger\hat{\sigma}_- + ig\hbar(\hat{\mathbf{a}}\hat{\sigma}_-^\dagger - \hat{\sigma}_-), \tag{11.2}$$

where $\hat{\sigma}_-$ is the lowering operator for transition $\mu_\uparrow$, ω_c and ω_x are the resonance frequencies of the cavity mode and transition $\mu_\uparrow$ respectively, and g is the coupling strength between the cavity mode and transition $\mu_\uparrow$. In the weak excitation limit, the Heisenberg-Langevin equations are [49–51]

$$\frac{d\hat{\mathbf{a}}}{dt} = -\Big[i(\omega_c - \omega) + \frac{\kappa}{2}\Big]\hat{\mathbf{a}} - ig\hat{\sigma}_- + \sqrt{\kappa_{ex}}\hat{\mathbf{a}}_{\mathbf{in}} \tag{11.3}$$

$$\frac{d\hat{\mathbf{\sigma}}_-}{dt} = -\Big[i(\omega_x - \omega) + \gamma\Big]\hat{\sigma}_- - ig\hat{\mathbf{a}}, \tag{11.4}$$

where κ is the total cavity energy delay rate given by $\kappa = \kappa_{ex} + \kappa_i$, κ_i is the intrinsic loss rate of the cavity due to material absorption and coupling to undesired leaky modes, and γ is the dipole decay rate of for transition $\mu_\uparrow$.

We calculate the cavity field operator by taking the steady solution of (11.3) and (11.4). When the spin is in spin-down state, we have $\langle\hat{\sigma}_-\rangle = 0$, therefore the steady solution for $\hat{\mathbf{a}}$ can be calculated from (11.3) and is given by

$$\langle\hat{\mathbf{a}}\rangle = \frac{\sqrt{\kappa_{ex}}\langle\hat{\mathbf{a}}_{\mathbf{in}}\rangle}{i(\omega_c - \omega) + \frac{\kappa}{2}}. \tag{11.5}$$

When the spin is in spin-up state, the expression for $\langle\hat{\mathbf{a}}\rangle$ is given by

$$\langle\hat{\mathbf{a}}\rangle = \frac{\sqrt{\kappa_{ex}}\big[i(\omega_x - \omega) + \gamma\big]}{\big[i(\omega_c - \omega) + \frac{\kappa}{2}\big]\big[i(\omega_x - \omega) + \gamma\big] + g^2}\langle\hat{\mathbf{a}}_{\mathbf{in}}\rangle. \tag{11.6}$$

We calculate the cavity reflection coefficients $r_\downarrow$ and $r_\uparrow$ for both the spin-down and spin-up cases by combining (11.5) or (11.6) with (11.1). For the spin-down case, we obtain $\langle\hat{\mathbf{a}}_{\mathbf{out}}\rangle = r_\downarrow\langle\hat{\mathbf{a}}_{\mathbf{in}}\rangle$, where $r_\downarrow$ is given by,

$$r_\downarrow = 1 - \frac{\alpha\kappa}{i(\omega_c - \omega) + \frac{\kappa}{2}}, \tag{11.7}$$

where α is the interference contrast given by $\alpha = \kappa_{ex}/\kappa$. For the spin-up case, we obtain $\langle\hat{\mathbf{a}}_{\mathbf{out}}\rangle = r_\uparrow\langle\hat{\mathbf{a}}_{\mathbf{in}}\rangle$, where $r_\uparrow$ is given by

$$r_\uparrow = 1 - \frac{\alpha\kappa\big[i(\omega_x - \omega) + \gamma\big]}{\big[i(\omega_c - \omega) + \frac{\kappa}{2}\big]\big[i(\omega_x - \omega) + \gamma\big] + g^2}. \tag{11.8}$$

11.2.2 Resonance Case: A Spin-Photon Quantum Switch

We focus on the resonance condition where $\omega = \omega_c = \omega_x$. In this case, the cavity reflection coefficients simplify to

$$r_\downarrow = 1 - 2\alpha \tag{11.9}$$

$$r_\uparrow = 1 - \frac{2\alpha}{1+C}, \tag{11.10}$$

where C is the cooperativity of the system given by $C = 2g^2/\kappa\gamma$.

When $\alpha > 0.5$ and $C > 2\alpha - 1$, $r_\uparrow$ and $r_\downarrow$ have opposite signs. Thus, the spin state conditionally shifts the phase of a reflected photon by π, implementing a quantum phase operation. An ideal phase switch would be attained in the limit of large cooperativity ($C \gg 1$) and a perfect single-sided cavity ($\alpha = 1$) where the reflection coefficient becomes $r_\downarrow = -1$ and $r_\uparrow = 1$.

The quantum phase switch allows one qubit to conditionally switch the other qubit between its two orthogonal eigenstates. We consider the case where the polarization state of the photon encodes quantum information. We assume that the cavity mode has a well defined polarization direction $\hat{y}$. Therefore only a y-polarized photon experiences spin-dependent phase shift upon reflection, whereas an x-polarized incident photon does not couple to the cavity and gets directly reflected without a phase shift. If the cavity mode does not have a well-defined polarization (i.e. the cavity supports polarization degenerate modes), we could use a simple polarization interferometry setup as illustrated in Fig. 11.2 to implement the similar idea.

We express the state of a photon incident on the cavity in the basis states $|x\rangle$ and $|y\rangle$, which denote the polarization states oriented orthogonal and parallel to the cavity mode respectively. For a right-circularly-polarized incident photon $|x\rangle + i\,|y\rangle$, the reflected state is given by $|x\rangle + i r_{\uparrow(\downarrow)}\,|y\rangle$ (before renormalization). In the limit of large cooperativity and perfect single-sided cavity, the state of the reflected photon remains right-circularly polarized if the atom is in the spin-up state, but becomes left-circularly polarized for spin-down. Similarly, a single control photon can flip the state of the spin. If the spin is prepared in the state $|\uparrow\rangle + |\downarrow\rangle$, then after a

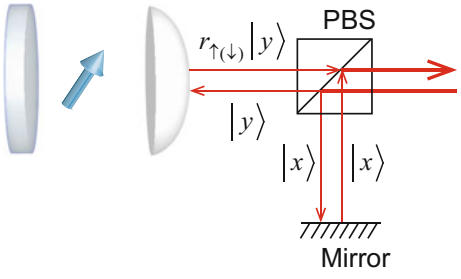

Fig. 11.2 Schematic setup to implement a spin-photon quantum switch where the polarization states of the photon encode quantum information

y-polarized photon reflects from the cavity the spin-state transforms to $|\uparrow\rangle - |\downarrow\rangle$, but an x-polarized photon does not flip the spin.

We note that when $\alpha > 0.5$ but $C < 2\alpha - 1$, $r_\uparrow$ and $r_\downarrow$ have the same sign. Thus the quantum phase operation is not available for a resonant photon if the system cooperativity is too low.

11.2.3 Detuned Case: Spin-Dependent Kerr Rotation

The general expression for $r_\downarrow$ and $r_\uparrow$ are given by (11.7) and (11.8) respectively. We can rewrite $r_{\downarrow(\uparrow)}$ as $r_{\downarrow(\uparrow)} = |r_{\downarrow(\uparrow)}|e^{i\phi_{\downarrow(\uparrow)}}$, where $\phi_{\downarrow(\uparrow)}$ represents the phase of the reflection coefficient $r_{\downarrow(\uparrow)}$. Since in general $\phi_\downarrow \neq \phi_\uparrow$, the spin can still apply spin-dependent phase shift on the photon. The phase difference between the spin-up and spin-down state ϕ is given by $\phi = \phi_\downarrow - \phi_\uparrow$, which is typically nonzero but not necessarily π any more.

The nonzero value of ϕ can be utilized to realize spin-dependent Kerr rotation of a photon, as demonstrated in [45, 46]. Assuming the polarization of the incident photon is in the state $|x\rangle + i\,|y\rangle$, the reflected state becomes $|P_{\uparrow(\downarrow)}\rangle = |x\rangle + i|r_{\uparrow(\downarrow)}|e^{i\phi_{\uparrow(\downarrow)}}\,|y\rangle$ (before renormalization). Therefore, the polarizations of the reflected photon are different for the spin-up and spin-down cases, as long as $\langle P_\uparrow|P_\downarrow\rangle \neq 1$, which is equivalent to $\phi \neq 0$.

Similarly, a single detuned photon can also rotate the state of the spin. If the spin is prepared in the state $|\uparrow\rangle + |\downarrow\rangle$, then after a y-polarized photon reflects from the cavity the spin-state transforms to $|r_\uparrow|\,|\uparrow\rangle + |r_\downarrow|e^{i\phi}\,|\downarrow\rangle$ (after taking out an overall phase factor). If $|r_\uparrow| \simeq |r_\uparrow|$, this operation corresponds to the rotation of the spin Bloch vector by an angle ϕ along the equator of the spin Bloch sphere.

For the detuned case, we do not require the cooperativity to be greater than $2\alpha - 1$ in order to induce spin-dependent phase shift. Indeed [45] demonstrated spin-dependent Kerr rotation of a photon with a coopeartivity of $C = 0.2$. However, there is still significant difference between the regime $C > 2\alpha - 1$ and $C < 2\alpha - 1$. Figure 11.3 shows numerically calculated phase shift ϕ as a function of the detuning

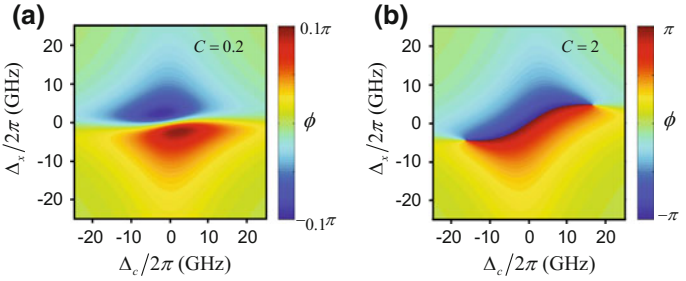

Fig. 11.3 Phase shift ϕ as a function of the detuning Δ_c and Δ_x. **a** $C = 0.2$. **b** $C = 2$

Δ_c and Δ_x, where we define $\Delta_c = \omega - \omega_c$ and $\Delta_x = \omega - \omega_x$. In both Fig. 11.3a, b, we use the following parameters from a realistic quantum dot based cavity QED system [47]: $\alpha = 0.8$, $\kappa/2\pi = 36$ GHz, $\gamma/2\pi = 3$ GHz. Figure 11.3a shows the case where we set $g/2\pi = 10.4$ GHz so that the cooperativity is $C = 2$ and satisfies $C > 2\alpha - 1$. Figure 11.3b shows the case where we set $g/2\pi = 3.3$ GHz so that the cooperativity is $C = 0.2$ and does not meet the condition $C > 2\alpha - 1$. For the case of $C = 2$, we are able to tune the phase shift ϕ to an arbitrary value between $-\pi$ and π, by simply controlling the detuning Δ_c and Δ_x. However, when the cooperativity is small, we can only tune the phase shift ϕ between $-\phi_{max}$ and ϕ_{max}, where $\phi_{max} < \pi$ is an upper limit that is determined by the system cooperativity. As an example, in Fig. 11.3a we have $\phi_{max} = 0.1\pi$.

11.3 Quantum Dot Spins in a Nanophotonic Cavity

Charged quantum dots exhibit spin-dependent optical transitions. As described in Sect. 11.2, by selectively coupling the spin-dependent optical transitions of a charged quantum dot to a cavity mode, one can induce strong interactions between the quantum dot spin and a photon. In this section, we review the experimental efforts to integrate quantum dot spins with different nanophotonic cavities, including micropillar cavities and photonic crystal cavities.

11.3.1 Micropillar Cavities

A micropillar cavity is formed by two Bragg reflectors, which are made of alternative layers GaAs and AlAs. The diameter of the pillar is typically in the order of several micron meters, which lead to a highly localized mode with mode volume in the order of $10(\lambda/n)^3$. One can engineer the cavity transmittance and reflectance by designing the number of layers for the top and bottom Bragg reflector. For example, a single sided cavity can be created by introducing a highly reflective bottom mirror with more layers and an outcoupling top mirror with less layers.

In 2009, Rakher et al. firstly reported integration of a charge tunable quantum dot with a micropillar cavity [41]. The reported device achieves a cooperativity of $C = 2$, which enables significant cavity reflectivity modulation when an extra charge is loaded into the quantum dot. Spin-dependent coupling between a charged quantum dot and a micropillar cavity is reported in [45, 46]. Both works utilized a device with low cooperativity ($C < 0.2$), and observe spin-dependent Kerr rotation of a reflected photon with a polarization rotation degree of $\sim 6°$.

Micropillar cavities enable efficient coupling between an incident field and the cavity mode, because the cavity mode is well matched to a Gaussian mode in the far field. Recent works have demonstrated an input coupling efficiency of exceeding 95% [52], which is a very promising property for achieving deterministic spin-photon

interactions. However, coherent optical manipulation of the quantum dot spin in a micropillar cavity is yet to be demonstrated.

11.3.2 Photonic Crystal Cavities

Photonic crystals are periodic nanostructures fabricated on a dielectric material, which lead to periodic modulation of the refractive index in the length scale of an optical wavelength. In a photonic crystal, the motion of a photon obeys optical Bragg scattering, very similarly as the way an electron propagates in ionic lattices. In addition, one can engineer photonic crystals to open a photonic band gap, analogous to an electronic band gap in semiconductors, which prohibits the propagation of photons for certain directions within some frequency range.

Defects in a photonic crystal can support highly localized cavity modes within the photonic band gap, referred as photonic crystal cavities. These cavities support small mode volume (in the order of $(\lambda/n)^3$) and high quality factor, which enable strong light-matter interactions with an embedded quantum emitter [25, 28]. In addition, the properties of a photonic crystal cavity, such as the resonant frequency, mode profile, and polarization can be easily controlled by tailoring the geometry of the photonic crystals or the shape of the defect areas. Photonic crystal cavities can also be easily integrated with other cavities or waveguides using the scalable photonic crystal architecture [33, 53–56]. These assets make the photonic crystal cavity a very attractive platform for realizing integrated photonics.

Several groups have reported deterministic charging of a quantum dot embedded in a photonic crystal cavity [42, 43]. In 2013, Carter et al. firstly demonstrated coherent control of a quantum dot spin embedded in a photonic crystal cavity [44]. This work operated far in the weak coupling regime where the quantum dot produced a spin-dependent cavity reflectivity with contrast of less than 1%. In 2016, Sun et al. firstly demonstrated strong coherent spin-photon interactions based on a strongly coupled charged quantum dot and a photonic crystal cavity [47]. The device has a cooperativity of $C = 2$, enabling a quantum switch between a quantum dot spin and a photon. We will review this work in details in Sect. 11.4.

11.4 Experimental Demonstrations of a Spin-Photon Quantum Switch

In this chapter, we discuss experimental demonstrations of a spin-photon quantum switch using a strongly coupled charged quantum dot and a photonic crystal cavity. We utilized a negatively charged quantum dot containing a single electron. In the presence of a magnetic field applied in the Voigt geometry, the energy structure of the quantum dot is shown in Fig. 11.4. The states of the dot include two ground states,

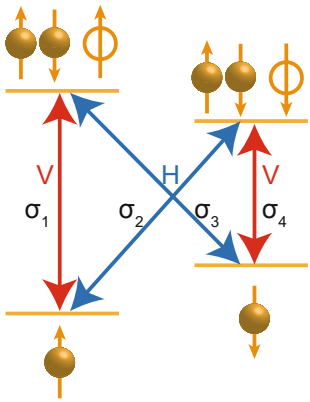

Fig. 11.4 Energy level structure of a charged quantum dot with an external magnetic field applied in the Voigt configuration

corresponding to the two electron spin orientations, and two excited trion states that optically couple to the ground states via four optical transitions denoted as $\sigma_1 - \sigma_4$. The energy level structure consists of two λ-systems and is slightly different from the single λ-system described in Fig. 11.1b. However, we can still induce spin-dependent cavity reflectivity by resonantly coupling only transition σ_1 with the cavity mode, and decoupling all other transitions from the cavity by a large magnetic field induced detuning. Thus, the quantum dot resonantly couples to the cavity only when it is in the spin-up state, inducing a spin-dependent reflection coefficient. As described in Sect. 11.2.2, we are able to realize a quantum switch by utilizing the spin-dependent reflection coefficients.

11.4.1 Device Characterization

To characterize the device, we mount the sample in a closed-cycle liquid-helium cryostat and cool it down to 3.6 K. The sample mount is placed inside the bore of a superconducting magnet that can apply magnetic fields up to 9.2 T. The sample is oriented such that the magnetic field is in the in-plane direction (Voigt configuration), and the cavity axis is approximately 45° with respect to the magnetic field. Sample excitation and collection is performed with a confocal microscope using an objective lens with numerical aperture of 0.68. The coupling efficiency for this configuration is measured to be 1% by measuring the Stark shift of the quantum dot under cavity-resonant excitation [57].

We identify a charged quantum dot coupled to the cavity from the photoluminescence spectrum of the device under a magnetic field applied in the Voigt configuration. Figure 11.5a shows the photoluminescence spectrum from the device used in our measurements when excited using an 860 nm continuous wave laser. At 0 T, the emission spectrum shows a bright peak due to the cavity (labeled as CM) and a second peak due to the quantum dot (labeled as QD), which is red-detuned from the

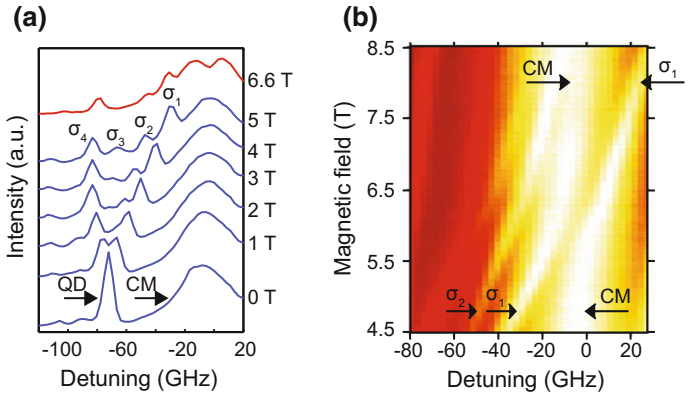

Fig. 11.5 Device characterization with photoluminescence. **a** Photoluminescence spectrum. The *blue lines* show the spectra at various magnetic fields ranging from 0 to 5 T. The *red line* shows the spectrum at 6.6 T, where transition σ_1 is resonant with the cavity. **b** Cavity photoluminescence as a function of the magnetic field

cavity resonance by 0.19 nm (67 GHz). As we increase the magnetic field, the quantum dot splits into four peaks corresponding to the four optical transitions shown in Fig. 11.4.

To demonstrate strong coupling between the quantum dot and the cavity, we finely tune the magnetic field over the range of 4.5–8.5 T and measure the cavity photoluminescence. Figure 11.5b shows the photoluminescence spectrum near the cavity resonance as a function of magnetic field. In this range, transition σ_1 tunes over the cavity resonance and exhibits an anti-crossing, indicating that the system operates in the strong coupling regime.

11.4.2 Spin-Dependent Cavity Reflectivity

To demonstrate that the spin can flip the state of the photon, we use the polarization interferometry set-up shown in Fig. 11.6. We excite the cavity with right-circularly polarized light, and measure the reflected signal along either the left-circularly or right-circularly polarized component. Figure 11.7 shows both the cross-polarized (red diamonds) and co-polarized reflection spectrum (blue circles) when the quantum dot is detuned from the cavity so that the two systems are decoupled. By fitting the reflection spectrum to a Lorentzian lineshape (blue and red solid lines), we determine the cavity energy decay rate to be $\kappa/2\pi = (35.9 \pm 0.7)$ GHz and the interference contrast to be $\alpha/2\pi = 0.81 \pm 0.01$.

We next apply a magnetic field of 6.6 T that tunes transition σ_1 onto cavity resonance via a Zeeman shift. We excite the quantum dot with a narrowband tunable laser to optically pump the spin state [58, 59]. We first tune the optical pumping

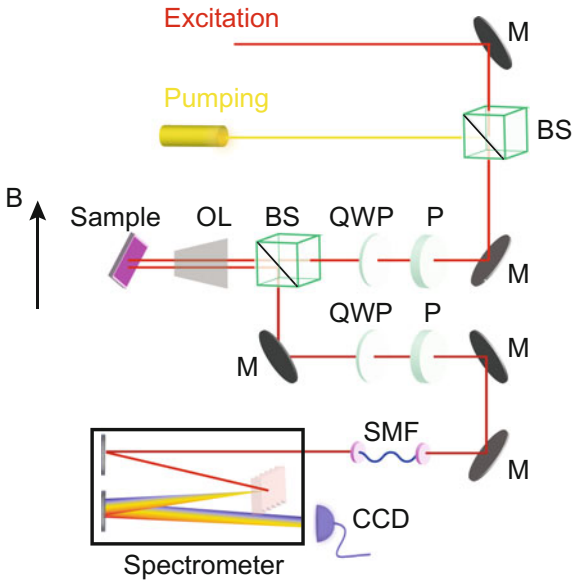

Fig. 11.6 Measurement setup. OL, objective lens; QWP, quarter wave plate; P, polarizer; BS, beam splitter; M, mirror; SMF, single mode fiber; CCD, charged coupled device

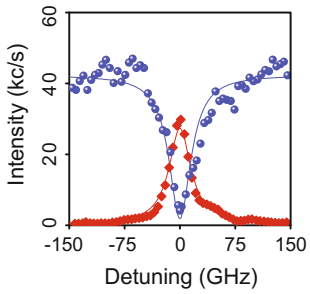

Fig. 11.7 Co-polarized (*blue circles*) and cross-polarized (*red diamonds*) cavity reflection spectrum with no magnetic field. *Blue* and *red solid lines* show the calculated spectrum (color figure online)

laser to transition σ_4 to prepare the quantum dot in the spin-up state. The blue circles in Fig. 11.8a show the cross-polarized reflection spectrum with the optical pumping laser, which exhibits a vacuum Rabi splitting. When we turn off the pumping laser, we observe a reduced contrast due to random spin fluctuations (red diamonds). In contrast, when we optically pump transition σ_2 to initialize the quantum dot to the spin-down state, we observe a spectrum that closely resembles a bare cavity (Fig. 11.8b). This spin-dependent reflection spectrum is one of the essential properties of the phase switch.

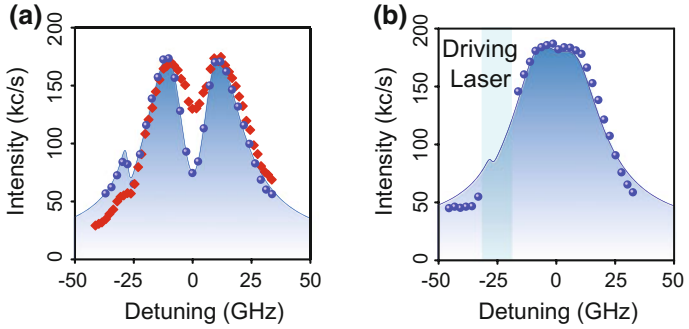

Fig. 11.8 Spin-dependent cavity reflectivity. **a** Cavity reflection spectrum under a 6.6 T magnetic field with (*blue circles*) and without (*red diamonds*) an optical pumping laser resonant with transition σ_4. The *blue solid line* shows the calculated spectrum for the case where the optical pumping laser is turned on. With the pumping laser, we observe a suppression of the cavity response at the σ_1 resonance due to strong coupling. We also observe a Fano-resonant lineshape at 27 GHz detuning, corresponding to the coupling between transition σ_2 and the cavity mode. **b** Cavity reflection spectrum when the pump laser is resonant with transition σ_2. The *blue circles* show the measured spectrum, and the *solid line* shows calculated spectrum. The center wavelength is 927.48 nm for all panels (color figure online)

11.4.3 Coherent Control of Cavity Reflectivity

To demonstrate control of a reflected photon using a coherently prepared spin state, we use all-optical coherent control to manipulate the spin. We fix the magnetic field at 6.6 T. A narrowband continuous-wave laser tuned to transition σ_4 performs spin initialization and circularly polarized picosecond optical pulses generate an effective spin rotation [13, 14]. We perform spin rotations using 6 ps rotation pulses with center frequencies detuned by 520 GHz from the cavity resonance (equal to 15 cavity linewidth). To rotate the spin over the Bloch sphere, we utilize the Ramsey interferometry setup illustrated in Fig. 11.9a, which generates a pair of rotation pulses separated by a time delay τ. A third laser pulse probes the cavity reflectivity a time Δt after the second rotation pulse. We attenuate this laser so that a single pulse contains an average of 0.12 photons coupled to the cavity to ensure a low probability of two-photon events. We set the power of the continuous-wave optical pumping laser to 30 nW. At this power we measure a spin initialization time of (1.27 ± 0.09) ns, which is slow compared with τ and Δt, but fast compared with the repetition time of the experiment (13 ns).

Figure 11.9b shows the reflected probe intensity as a function of rotation pulse power P and delay τ, where we set Δt to 140 ps. We observe Ramsey oscillations in the reflected probe intensity as a function of both P and τ. Figure 11.9c plots the emission intensity of the quantum dot at transition σ_2 for the same measurement, which provides a second readout of the spin state. We observe the same Ramsey oscillation pattern in the quantum dot emission signal, confirming that the reflection modulation shown in Fig. 11.9b is induced by coherent spin manipulation. Figure 11.9d

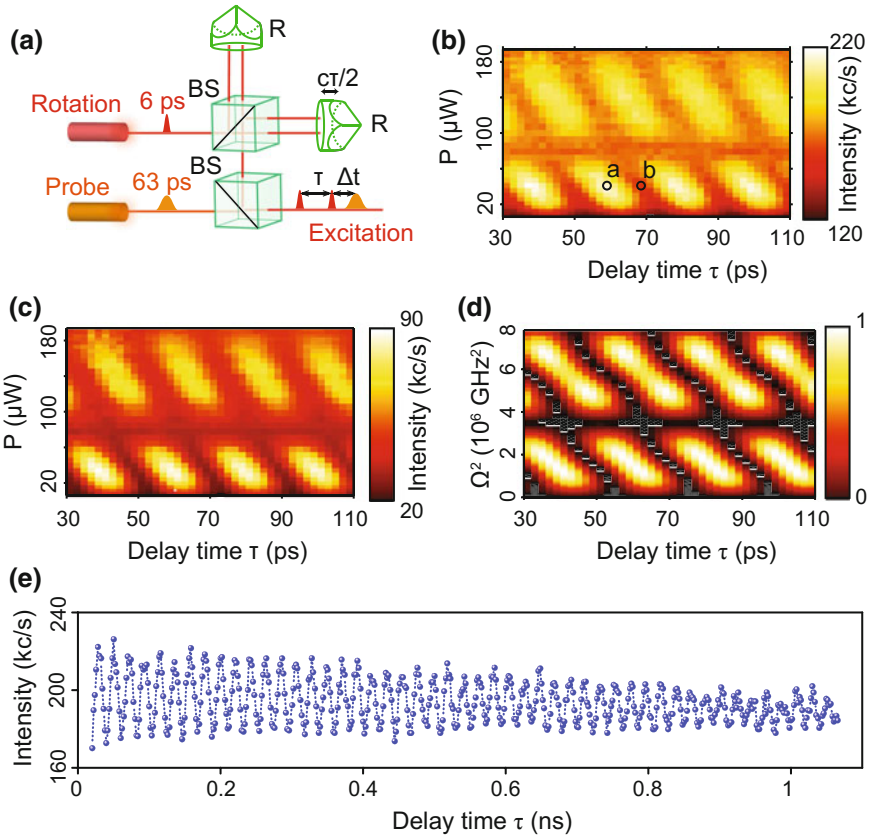

Fig. 11.9 Ramsey interference measurements. **a** Experimental setup for generating the Ramsey pulse sequence. The delay time τ between the two rotation pulses is controlled by a movable retro-reflector mounted on a computer-controlled translation stage. BS, beam splitter; R, retro-reflector. **b** Reflected probe intensity as a function of rotation pulse power P and the delay time τ. **c** Intensity of the quantum dot emission at σ_2 transition frequency as a function of rotation pulse power P and the delay time τ. **d** Calculated spin-down state population as a function of peak rotation pulse power and the delay time τ. We express the rotation pulse as a classical time-varying Rabi frequency with a Gaussian pulse shape and peak power Ω^2. **e** Reflected probe intensity as a function of delay time τ

shows the numerically calculated value for the population of the spin-down state for comparison, which exhibit good agreement with experiments.

In Fig. 11.9e we plot the reflected probe intensity over a larger time range of 1 ns. We fix the power of each rotation pulse to 40 μW, which corresponds to a $\pi/2$-rotation. From the decay of the fringe visibility, we calculate a $T_2^\star$ time of (0.94 ± 0.02) ns. This coherence time is limited by inhomogeneous broadening due to a slowly fluctuating nuclear spin background [11], along with decoherence due to continuous optical pumping during the rotation pulse sequence. We could reduce

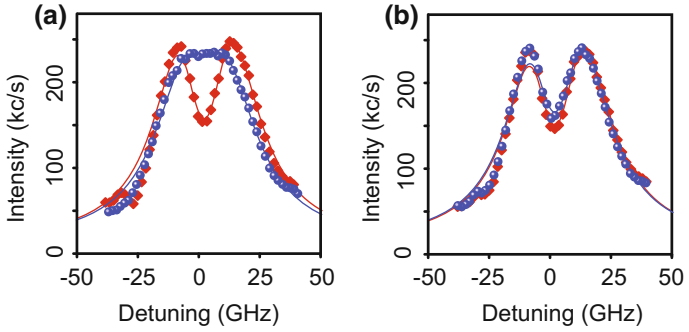

Fig. 11.10 Time-resolved cavity reflection spectrum. **a** and **b**, Reflected probe intensity as a function of probe detuning at the rotation condition indicated by point *a* and point *b* in Fig. 11.9b respectively. *Blue circles* are $\Delta t = 140$ ps; *red diamonds* are $\Delta t = 13$ ns. *Solid lines* are the calculated spectra. The center wavelength is 927.48 nm for both spectra (color figure online)

these effects by turning off the pump laser during the measurement process and using a nuclear field locking [11] or spin echo technique [12], which has been shown to improve the coherence to up to 2.6 μs.

To characterize the fidelity of the spin state preparation, we tune the probe laser across the cavity resonance while setting P and τ to the conditions indicated by the circles in Fig. 11.9b. The resulting cavity spectra are plotted in Fig. 11.10. In Fig. 11.10a the two pulses arrive in-phase with the Larmor precession of the spin, and the quantum dot rotates to the spin-down state. The cavity spectrum (blue circles) is thus similar to the bare cavity Lorentzian lineshape. Figure 11.10b shows the case where the two rotation pulses arrive out-of-phase and the quantum dot rotates back to the spin-up state. The cavity (blue circles) now exhibits a strongly coupled spectrum. We also plot the measured spectrum when $\Delta t = 13$ ns (red diamonds) for comparison. At this condition the spin is re-initialized to the spin-up state in both cases.

11.4.4 Controlling a Spin with a Photon

The previous measurements demonstrate that the spin state of the quantum dot induces a conditional phase shift on the photon. A quantum phase switch would also exhibit the complementary effect, where reflection of a single photon rotates the spin state. To demonstrate this phase shift, we use the experimental configuration shown in Fig. 11.11a. We again perform a Ramsey interference measurement but we inject a weak laser pulse that serves as the control field before the second rotation pulse arrives. We generate the control pulse in the same way as the probe pulse in the previous measurement, with pulse duration of 63 ps. When a control photon couples

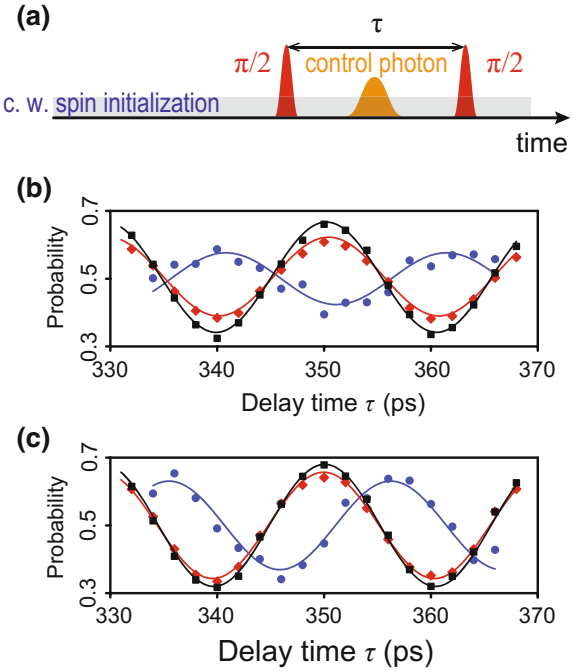

Fig. 11.11 Photon-induced spin phase switch. **a** Pulse timing diagram showing the relative time delays between the rotation pulses and the control field. **b** Occupation probability of the spin-down state as a function of the delay time τ, in the absence of control pulse (*black squares*), conditioned on detecting a reflected control photon polarized along the cavity axis (*blue circles*), and in the presence of the control field but not conditioning on the detection of a control photon (*red diamonds*). The control field is resonant with the σ_1 quantum dot transition. **c** Same as **b**, except that the control field is *blue detuned* from the σ_1 quantum dot transition (color figure online)

to the cavity, it imposes a phase shift on the spin-down state, which shifts the phase of the Ramsey fringes.

We perform statistical spin readout by monitoring the emission at the σ_2 frequency. The blue circles in Fig. 11.11b show the occupation probability of the spin-down state conditioned on the detection of a control photon, as a function of delay between the two rotation pulses. These data are obtained by performing a two photon correlation measurement. The blue solid line is a numerical fit to a sinusoidal function. We compare this curve to the occupation probability of the spin-down state when we block the control field (black squares with black line as a numerical fit). The interference fringe conditioned on detecting a single control photon is shifted in phase by $(1.09 \pm 0.09)\pi$ radians relative to the case where there is no control photon, demonstrating that a single control photon applies a large phase shift to the spin. We attribute the degraded visibility of the Ramsey fringe conditioned on a control photon to finite cooperativity, intrinsic cavity losses and occasional two-photon incidence events.

We can tune the phase shift imparted on the spin by a control photon by introducing a frequency detuning between the control field and transition σ_1, which enables us to apply arbitrary controlled phase shifts. Figure 11.11c shows the same measurement for a blue detuned control field. The conditioned data (blue circles) show a $(0.59 \pm 0.05)\pi$ radian phase shift, which corresponds to a detuning of 7.3 GHz. We also plot the occupation probability of the spin-down state in the presence of the control field but without conditioning on the detection of the control photon (red diamonds in Fig. 11.11b, c). These curves are very similar to the case where the control field is blocked, which indicates that the average number of control photons per pulse coupled to the cavity is much smaller than one.

11.5 Discussions and Outlooks

In this chapter, we reviewed recent experimental progress on interfacing a single quantum dot spin and a single photon using a nanophotonic cavity QED system. Especially, we introduced an experiment that demonstrated a spin-photon quantum phase switch, which achieves strong coherent interactions between a single quantum dot spin and a photon. The strong light-matter coupling strength of quantum dot based cavity QED devices enables a quantum switch operating at unprecedented bandwidths, where the spin can switch photon wavepackets as short as tens of picoseconds [47]. Perhaps the most intriguing aspect of the spin-photon quantum switch is that it monolithically combines spins with strongly interacting nanophotonic structures on a single semiconductor chip, which may have many beneficial properties for future integration and scalability.

The demonstrated spin-photon quantum switch could enable lots of applications in quantum information processing. Recent theory works have showed the potential to deterministically generate spin-photon entanglement based on a similar quantum dot based cavity QED system [60], which is an important step towards solid-state implementations of quantum repeaters and quantum networks. The spin-photon quantum interface might also enable single-shot optical readout of a quantum dot spin in the Voigt configuration [61], an extremely challenging task for quantum dot based quantum information processing. The ultimate direction for this research direction is to construct integrated quantum photonic circuits and on-chip quantum processors using nanophotonic platform with solid-state spins embedded.

Another important aspects of the future works is to improve the performance of the cavity device. Cavity designs with smaller mode-volume could improve the system cooperativity [62, 63], thus enable higher switching fidelity. Using delta-doping layers [14] or active charge stabilization [44] could further improve the spin state preparation fidelity. The spin-photon quantum switch results can also be directly applied in waveguide integrated devices that are more conducive to on-chip integration and can exhibit similar strong light-matter interactions [54]. In such on-chip implementations, waveguide losses create further challenges by degrading the cavity quality factor, which would reduce the cooperativity. Waveguide-coupled devices

would therefore require higher bare cavity quality factor to ensure that the light remains on the chip. Past work has demonstrated a quality factor exceeding 50,000 using GaAs photonic crystal cavities operating at near-infrared wavelengths [64], and quality factor exceeding 250,000 in cavities operating at a longer wavelength [65], which could potentially enable both efficient on-chip coupling and high cooperativity. Employing regulated quantum dot growth techniques [66, 67] in conjunction with local frequency tuning [57] could further open up the possibility to integrate multiple quantum dot spins on a single semiconductor chip.

References

1. J.I. Cirac, P. Zoller, H.J. Kimble, H. Mabuchi, Quantum state transfer and entanglement distribution among distant nodes in a quantum network. Phys. Rev. Lett. **78**(16), 3221 (1997)
2. H. Jeff Kimble, The quantum internet. Nature **453**(7198), 1023–1030 (2008)
3. J.I. Cirac, A.K. Ekert, S.F. Huelga, C. Macchiavello, Distributed quantum computation over noisy channels. Phys. Rev. A **59**(6), 4249 (1999)
4. J. Cho, H.-W. Lee, Generation of atomic cluster states through the cavity input-output process. Phys. Rev. Lett. **95**(16), 160501 (2005)
5. S. Ritter, C. Nölleke, C. Hahn, A. Reiserer, A. Neuzner, M. Uphoff, M. Mücke, E. Figueroa, J. Bochmann, G. Rempe, An elementary quantum network of single atoms in optical cavities. Nature **484**(7393), 195–200 (2012)
6. J. Volz, R. Gehr, G. Dubois, J. Estève, J. Reichel, Measurement of the internal state of a single atom without energy exchange. Nature **475**(7355), 210–213 (2011)
7. A. Reiserer, S. Ritter, G. Rempe, Nondestructive detection of an optical photon. Science **342**(6164), 1349–1351 (2013)
8. T.G. Tiecke, J.D. Thompson, N.P. de Leon, L.R. Liu, V. Vuletić, M.D. Lukin, Nanophotonic quantum phase switch with a single atom. Nature **508**(7495), 241–244 (2014)
9. L.-M. Duan, H.J. Kimble, Scalable photonic quantum computation through cavity-assisted interactions. Phys. Rev. Lett. **92**(12), 127902 (2004)
10. A. Reiserer, N. Kalb, G. Rempe, S. Ritter, A quantum gate between a flying optical photon and a single trapped atom. Nature **508**(7495), 237–240 (2014)
11. X. Xiaodong, W. Yao, B. Sun, D.G. Steel, A.S. Bracker, D. Gammon, L.J. Sham, Optically controlled locking of the nuclear field via coherent dark-state spectroscopy. Nature **459**(7250), 1105–1109 (2009)
12. D. Press, K. De Greve, P.L. McMahon, T.D. Ladd, B. Friess, C. Schneider, M. Kamp, S. Höfling, A. Forchel, Y. Yamamoto, Ultrafast optical spin echo in a single quantum dot. Nat. Photonics **4**(6), 367–370 (2010)
13. J. Berezovsky, M.H. Mikkelsen, N.G. Stoltz, L.A. Coldren, D.D. Awschalom, Picosecond coherent optical manipulation of a single electron spin in a quantum dot. Science **320**(5874), 349–352 (2008)
14. D. Press, T.D. Ladd, B. Zhang, Y. Yamamoto, Complete quantum control of a single quantum dot spin using ultrafast optical pulses. Nature **456**(7219), 218–221 (2008)
15. E.D. Kim, K. Truex, X. Xu, B. Sun, D.G. Steel, A.S. Bracker, D. Gammon, L.J. Sham, Fast spin rotations by optically controlled geometric phases in a charge-tunable inas quantum dot. Phys. Rev. Lett. **104**(16), 167401 (2010)
16. K. De Greve, P.L. McMahon, D. Press, T.D. Ladd, D. Bisping, C. Schneider, M. Kamp, L. Worschech, S. Höfling, A. Forchel et al., Ultrafast coherent control and suppressed nuclear feedback of a single quantum dot hole qubit. Nat. Phys. **7**(11), 872–878 (2011)

17. T.M. Godden, J.H. Quilter, A.J. Ramsay, Y. Wu, P. Brereton, S.J. Boyle, I.J. Luxmoore, J. Puebla-Nunez, A.M. Fox, M.S. Skolnick, Coherent optical control of the spin of a single hole in an inas/gaas quantum dot. Phys. Rev. Lett. **108**(1), 017402 (2012)
18. Y. He, Y.-J. Yu-Ming He, X.J. Wei, M.-C. Chen, F.-L. Xiong, Y. Zhao, C. Schneider, M. Kamp, S. Höfling et al., Indistinguishable tunable single photons emitted by spin-flip raman transitions in ingaas quantum dots. Phys. Rev. Lett. **111**(23), 237403 (2013)
19. K. De Greve, Y. Leo, P.L. McMahon, J.S. Pelc, C.M. Natarajan, N.Y. Kim, E. Abe, S. Maier, C. Schneider, M. Kamp et al., Quantum-dot spin-photon entanglement via frequency down-conversion to telecom wavelength. Nature **491**(7424), 421–425 (2012)
20. W.B. Gao, P. Fallahi, E. Togan, J. Miguel-Sánchez, A. Imamoglu, Observation of entanglement between a quantum dot spin and a single photon. Nature **491**(7424), 426–430 (2012)
21. J.R. Schaibley, A.P. Burgers, G.A. McCracken, L.-M. Duan, P.R. Berman, D.G. Steel, A.S. Bracker, D. Gammon, L.J. Sham, Demonstration of quantum entanglement between a single electron spin confined to an inas quantum dot and a photon. Phys. Rev. Lett. **110**(16), 167401 (2013)
22. K. De Greve, P.L. McMahon, Yu. Leo, J.S. Pelc, C. Jones, C.M. Natarajan, N.Y. Kim, E. Abe, S. Maier, C. Schneider, et al., Complete tomography of a high-fidelity solid-state entangled spin-photon qubit pair. Nat. Commun. **4**, (2013)
23. W.B. Gao, P. Fallahi, E. Togan, A. Delteil, Y.S. Chin, J. Miguel-Sanchez, A. Imamoğlu, Quantum teleportation from a propagating photon to a solid-state spin qubit. Nat. Commun. **4** (2013)
24. A. Delteil, Z. Sun, W.-b. Gao, E. Togan, S. Faelt, A. Imamoglu, Generation of heralded entanglement between distant hole spins. Nat. Phys. (2015)
25. T. Yoshie, A. Scherer, J. Hendrickson, G. Khitrova, H.M. Gibbs, G. Rupper, C. Ell, O.B. Shchekin, D.G. Deppe, Vacuum rabi splitting with a single quantum dot in a photonic crystal nanocavity. Nature **432**(7014), 200–203 (2004)
26. J.P. Reithmaier, G. Sek, A. Löffler, C. Hofmann, S. Kuhn, S. Reitzenstein, L.V. Keldysh, V.D. Kulakovskii, T.L. Reinecke, A. Forchel, Strong coupling in a single quantum dot-semiconductor microcavity system. Nature **432**(7014), 197–200 (2004)
27. E. Peter, P. Senellart, D. Martrou, A. Lemaître, J. Hours, J.M. Gérard, J. Bloch, Exciton-photon strong-coupling regime for a single quantum dot embedded in a microcavity. Phys. Rev. Lett. **95**(6), 067401 (2005)
28. K. Hennessy, A. Badolato, M. Winger, D. Gerace, M. Atatüre, S. Gulde, S. Fält, E.L. Hu, A. Imamoğlu, Quantum nature of a strongly coupled single quantum dot-cavity system. Nature **445**(7130), 896–899 (2007)
29. D. Englund, A. Faraon, B. Zhang, Y. Yamamoto, J. Vučković, Generation and transfer of single photons on a photonic crystal chip. Opt. Express **15**(9), 5550–5558 (2007)
30. A. Faraon, A. Majumdar, D. Englund, E. Kim, M. Bajcsy, J. Vučković, Integrated quantum optical networks based on quantum dots and photonic crystals. New J. Phys. **13**(5), 055025 (2011)
31. D. Englund, A. Faraon, I. Fushman, N. Stoltz, P. Petroff, J. Vučković, Controlling cavity reflectivity with a single quantum dot. Nature **450**(7171), 857–861 (2007)
32. D. Englund, A. Majumdar, M. Bajcsy, A. Faraon, P. Petroff, J. Vučković, Ultrafast photon-photon interaction in a strongly coupled quantum dot-cavity system. Phys. Rev. Lett. **108**(9), 093604 (2012)
33. R. Bose, D. Sridharan, H. Kim, G.S. Solomon, E. Waks, Low-photon-number optical switching with a single quantum dot coupled to a photonic crystal cavity. Phys. Rev. Lett. **108**(22), 227402 (2012)
34. T. Volz, A. Reinhard, M. Winger, A. Badolato, K.J. Hennessy, E.L. Hu, A. Imamoğlu, Ultrafast all-optical switching by single photons. Nat. Photonics **6**(9), 605–609 (2012)
35. K. Srinivasan, O. Painter, Linear and nonlinear optical spectroscopy of a strongly coupled microdisk-quantum dot system. Nature **450**(7171), 862–865 (2007)
36. I. Fushman, D. Englund, A. Faraon, N. Stoltz, P. Petroff, J. Vučković, Controlled phase shifts with a single quantum dot. Science **320**(5877), 769–772 (2008)

37. D. Gerace, H.E. Türeci, A. Imamoglu, V. Giovannetti, R. Fazio, The quantum-optical josephson interferometer. Nat. Phys. **5**(4), 281–284 (2009)
38. A. Faraon, I. Fushman, D. Englund, N. Stoltz, P. Petroff, J. Vučković, Coherent generation of non-classical light on a chip via photon-induced tunnelling and blockade. Nat. Phys. **4**(11), 859–863 (2008)
39. K. Müller, A. Rundquist, K.A. Fischer, T. Sarmiento, K.G. Lagoudakis, Y.A. Kelaita, C.S. Muñoz, E. del Valle, F.P. Laussy, J. Vučković, Coherent generation of nonclassical light on chip via detuned photon blockade. Phys. Rev. Lett. **114**(23), 233601 (2015)
40. H. Kim, R. Bose, T.C. Shen, G.S. Solomon, E. Waks, A quantum logic gate between a solid-state quantum bit and a photon. Nat. Photonics **7**(5), 373–377 (2013)
41. M.T. Rakher, N.G. Stoltz, L.A. Coldren, P.M. Petroff, D. Bouwmeester, Externally mode-matched cavity quantum electrodynamics with charge-tunable quantum dots. Phys. Rev. Lett. **102**(9), 097403 (2009)
42. D. Pinotsi, J.M. Sanchez, P. Fallahi, A. Badolato, A. Imamoglu, Charge controlled self-assembled quantum dots coupled to photonic crystal nanocavities. Photonics Nanostruct. Fundam. Appl. **10**(3), 256–262 (2012)
43. K.G. Lagoudakis, K. Fischer, T. Sarmiento, A. Majumdar, A. Rundquist, J. Lu, M. Bajcsy, J. Vučković, Deterministically charged quantum dots in photonic crystal nanoresonators for efficient spin-photon interfaces. New J. Phys. **15**(11), 113056 (2013)
44. S.G. Carter, T.M. Sweeney, M. Kim, C.S. Kim, D. Solenov, S.E. Economou, T.L. Reinecke, L. Yang, A.S. Bracker, D. Gammon, Quantum control of a spin qubit coupled to a photonic crystal cavity. Nat. Photonics **7**(4), 329–334 (2013)
45. C. Arnold, J. Demory, V. Loo, A. Lemaître, I. Sagnes, M. Glazov, O. Krebs, P. Voisin, P. Senellart, L. Lanco, Macroscopic rotation of photon polarization induced by a single spin. Nat. Commun. **6** (2015)
46. P. Androvitsaneas, A.B. Young, C. Schneider, S. Maier, M. Kamp, S. Höfling, S. Knauer, E. Harbord, C.Y. Hu, J.G. Rarity, R. Oulton, Charged quantum dot micropillar system for deterministic light-matter interactions. Phys. Rev. B **93**, 241409 (2016). Jun
47. S. Sun, H. Kim, G.S. Solomon, E. Waks, A quantum phase switch between a single solid-state spin and a photon. Nat. Nanotechnol. **11**(6), 539–544 (2016)
48. D.F. Walls, G.J. Milburn, *Quantum Optics* (Springer Science & Business Media, Heidelberg, 2007)
49. S. Hughes, H. Kamada, Single-quantum-dot strong coupling in a semiconductor photonic crystal nanocavity side coupled to a waveguide. Phys. Rev. B **70**(19), 195313 (2004)
50. E. Waks, J. Vuckovic, Dipole induced transparency in drop-filter cavity-waveguide systems. Phys. Rev. Lett. **96**(15), 153601 (2006)
51. J.-T. Shen, S. Fan et al., Theory of single-photon transport in a single-mode waveguide. i. coupling to a cavity containing a two-level atom. Phys. Rev. A **79**(2), 023837 (2009)
52. V. Giesz, N. Somaschi, G. Hornecker, T. Grange, B. Reznychenko, L. De Santis, J. Demory, C. Gomez, I. Sagnes, A. Lemaître, et al., Coherent manipulation of a solid-state artificial atom with few photons. Nat. Commun. **7** (2016)
53. A. Faraon, E. Waks, D. Englund, I. Fushman, J. Vučković, Efficient photonic crystal cavity-waveguide couplers. Appl. Phys. Lett. **90**(7), 073102 (2007)
54. R. Bose, D. Sridharan, G.S. Solomon, E. Waks, Observation of strong coupling through transmission modification of a cavity-coupled photonic crystal waveguide. Opt. Express **19**(6), 5398–5409 (2011)
55. T. Cai, R. Bose, G.S. Solomon, E. Waks, Controlled coupling of photonic crystal cavities using photochromic tuning. Appl. Phys. Lett. **102**(14), 141118 (2013)
56. A.Y. Piggott, K.G. Lagoudakis, T. Sarmiento, M. Bajcsy, G. Shambat, J. Vučković, Photo-oxidative tuning of individual and coupled gaas photonic crystal cavities. Opt. Express **22**(12), 15017–15023 (2014)
57. R. Bose, D. Sridharan, G.S. Solomon, E. Waks, Large optical stark shifts in semiconductor quantum dots coupled to photonic crystal cavities. Appl. Phys. Lett. **98**(12), 121109 (2011)

58. C. Emary, X. Xu, D.G. Steel, S. Saikin, L.J. Sham, Fast initialization of the spin state of an electron in a quantum dot in the voigt configuration. Phys. Rev. Lett. **98**(4), 047401 (2007)
59. X. Xiaodong, W. Yanwen, B. Sun, Q. Huang, J. Cheng, D.G. Steel, A.S. Bracker, D. Gammon, C. Emary, L.J. Sham, Fast spin state initialization in a singly charged inas-gaas quantum dot by optical cooling. Phys. Rev. Lett. **99**(9), 097401 (2007)
60. S. Sun, E. Waks, Deterministic generation of entanglement between a quantum-dot spin and a photon. Phys. Rev. A **90**(4), 042322 (2014)
61. S. Sun, E. Waks, Single-shot optical readout of a quantum bit using cavity quantum electrodynamics. Phys. Rev. A **94**, 012307 (2016). Jul
62. Y. Ota, M. Shirane, M. Nomura, N. Kumagai, S. Ishida, S. Iwamoto, S. Yorozu, Y. Arakawa, Vacuum rabi splitting with a single quantum dot embedded in a h1 photonic crystal nanocavity. Appl. Phys. Lett. **94**(3), 3102 (2009)
63. R. Ohta, Y. Ota, M. Nomura, N. Kumagai, S. Ishida, S. Iwamoto, Y. Arakawa, Strong coupling between a photonic crystal nanobeam cavity and a single quantum dot. Appl. Phys. Lett. **98**(17), 3104 (2011)
64. E. Weidner, S. Combrié, A. De Rossi, J. Nagle, S. Cassette, A. Talneau, H. Benisty et al., Achievement of ultrahigh quality factors in gaas photonic crystal membrane nanocavity. Appl. Phys. Lett. **89**(22), 221104 (2006)
65. S. Combrié, A. De Rossi, Q.V. Tran, H. Benisty, Gaas photonic crystal cavity with ultrahigh q: microwatt nonlinearity at 1.55 μm. Opt. Lett. **33**(16), 1908–1910 (2008)
66. C. Schneider, M. Strauß, T. Sünner, A. Huggenberger, D. Wiener, S. Reitzenstein, M. Kamp, S. Höfling, A. Forchel, Lithographic alignment to site-controlled quantum dots for device integration. Appl. Phys. Lett. **92**(18), 183101 (2008)
67. M.K. Yakes, L. Yang, A.S. Bracker, T.M. Sweeney, P.G. Brereton, M. Kim, C.S. Kim, P.M. Vora, D. Park, S.G. Carter et al., Leveraging crystal anisotropy for deterministic growth of inas quantum dots with narrow optical linewidths. Nano Lett. **13**(10), 4870–4875 (2013)